Virology 500 (2017) 161–168

Contents lists available at ScienceDirect

Virology

journal homepage: www.elsevier.com/locate/yviro

Dynamic conformational changes in the rhesus TRIM5α dimer dictate the potency of HIV-1 restriction

Rajan Lamichhane[a], Santanu Mukherjee[b], Nikolai Smolin[c], Raymond F. Pauszek III[a], Margret Bradley[b], Jaya Sastri[d], Seth L. Robia[c], David Millar[a], Edward M. Campbell[b,*]

[a] Department of Integrative Structural and Computational Biology, The Scripps Research Institute, La Jolla, CA, USA
[b] Department of Microbiology and Immunology, Stritch School of Medicine, Loyola University Chicago, Chicago, IL, USA
[c] Department of Cell and Molecular Physiology, Stritch School of Medicine, Loyola University Chicago, Chicago, IL, USA
[d] Viral Mutation Section, HIV Dynamics and Replication Program, National Cancer Institute at Frederick, Frederick, MD, USA

ARTICLE INFO

Keywords:
Single molecule FRET
TRIM5alpha
HIV-1
Molecular dynamics simulation
smFRET
Restriction factor
Coiled coil
Dimer
Tripartite Motif

ABSTRACT

The TRIM5α protein from rhesus macaques (rhTRIM5α) mediates a potent inhibition of HIV-1 infection via a mechanism that involves the abortive disassembly of the viral core. We have demonstrated that alpha-helical elements within the Linker 2 (L2) region, which lies between the SPRY domain and the Coiled-Coil domain, influence the potency of restriction. Here, we utilize single-molecule FRET analysis to reveal that the L2 region of the TRIM5α dimer undergoes dynamic conformational changes, which results in the displacement of L2 regions by 25 angstroms relative to each other. Analysis of restriction enhancing or abrogating mutations in the L2 region reveal that restriction defective mutants are unable to undergo dynamic conformational changes and do not assume compact, alpha-helical conformations in the L2 region. These data suggest a model in which conformational changes in the L2 region mediate displacement of CA bound SPRY domains to induce the destabilization of assembled capsid during restriction.

1. Introduction

TRIM5α is a retroviral restriction factor which mediates a post-entry block to infection (Sastri and Campbell, 2011; Stremlau et al., 2004). The most well studied example of this restriction is the ability of the TRIM5α protein from rhesus macaques (rhTRIM5α) to potently inhibit HIV-1 infection (Sastri and Campbell, 2011; Stremlau et al., 2004). Like other members of the TRIM family of proteins, TRIM5α possesses the canonical RING, BBox2, and coiled coil (CC) domains that comprise the TRIpartite Motif that defines this family of proteins (Ozato et al., 2008). Like other TRIM family proteins, TRIM5α exhibits a strong tendency to self-associate into macromolecular assemblies in cells (Cai et al., 2008; Campbell et al., 2007). The N-terminal RING domain of TRIM5α is known to act as an E3 ubiquitin ligase (Pertel et al., 2011; Tareen and Emerman, 2011; Yamauchi et al., 2008; Yudina et al., 2015), and, together with the BBox2 domain, also functions to mediate the self-association of TRIM5α dimers (Diaz-Griffero et al., 2009; Li et al., 2011). The CC domain, in cooperation with the Linker 2 (L2) region, mediates the dimerization of TRIM5α monomers and the formation of higher order assemblies (Goldstone et al., 2014; Kar et al., 2011; Langelier et al., 2008; Sanchez et al., 2014; Sastri et al., 2010). TRIM5α also possesses a C-terminal SPRY domain, which is known to recognize determinants in the assembled viral core to mediate restriction (Ohkura et al., 2006; Stremlau et al., 2005; Yap et al., 2005). Following core binding, TRIM5α induces the abortive disassembly of the viral core (Stremlau et al., 2006; Zhao et al., 2011), although the mechanism by which this abortive disassembly is induced by TRIM5α remains poorly understood.

Structural studies have been valuable in understanding the molecular basis for the interactions between TRIM5α and the HIV-1 capsid (CA) core. Cryo-EM studies have revealed that TRIM5α can form hexagonal assemblies on artificially assembled CA lattices (Ganser-Pornillos et al., 2011; Li et al., 2016). The domain organization of TRIM5α within this assembly has recently been revealed by structural studies revealing that TRIM5α and TRIM25, a closely related TRIM family member, form relatively long antiparallel dimers (Goldstone et al., 2014; Sanchez et al., 2014) (Fig. 1B), the dimensions of which are consistent with these dimeric units spanning each face of the hexagonal lattice observed by cryo-EM (Ganser-Pornillos et al., 2011) (Fig. 1C). As such, the antiparallel dimer consisting of the CC-L2-SPRY domain are thought to represent the basic CA binding unit of TRIM5α, and recombinant proteins comprised of the CC-L2-SPRY domains have been observed to bind assembled CA in vitro (Zhao et al., 2011). Moreover, this minimal CA binding unit, lacking the N-terminal RING

* Corresponding author.

http://dx.doi.org/10.1016/j.virol.2016.10.003
Received 25 July 2016; Received in revised form 1 October 2016; Accepted 5 October 2016
0042-6822/ © 2016 Elsevier Inc. All rights reserved.

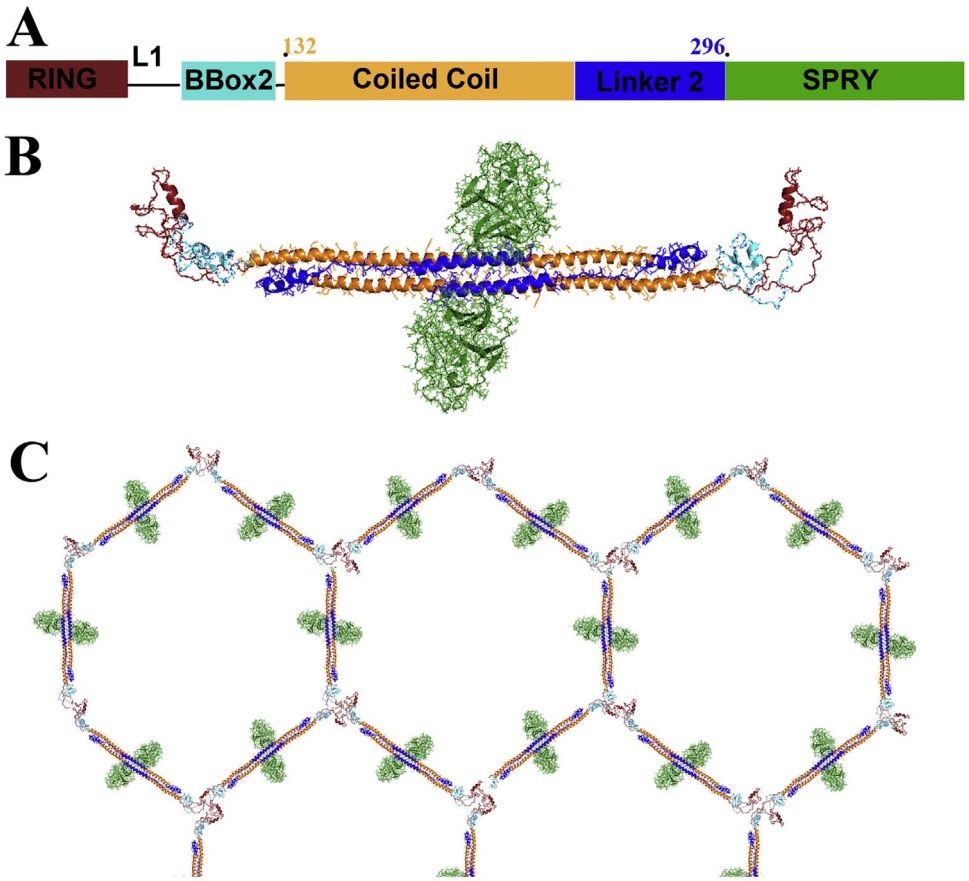

Fig. 1. Structural organization of TRIM5α assemblies: A. The domain structure of TRIM5α, with color coded domain structure used throughout the manuscript. B. Putative structure of TRIM5α dimer, assembled from a homology model of the CC-L2 dimer of rhTRIM5α and the structures of individual domains (Abe et al., 2007; Biris et al., 2012; Goldstone et al., 2014). C. Putative domain structures within hexagonal TRIM5α assembly (Ganser-Pornillos et al., 2011).

and BBox2 domains, exhibited the ability to disrupt CA tubes in vitro, suggesting that the minimal components of TRIM5α which induce the abortive disassembly of the viral core are located in the CC-L2-SPRY fragment of TRIM5α (Zhao et al., 2011). Although the mechanism underlying the disruption of assembled CA by the CC-L2-SPRY fragment was not determined, in the absence of enzymatic activity, one possibility is that dynamic changes in the conformation of these domains cooperatively induce CA disassembly. Consistent with this hypothesis, the recently published structure of the TRIM5α dimer failed to resolve a stretch of residues in the L2 region (Goldstone et al., 2014) which our studies have found to regulate the ability of rhTRIM5α to restrict HIV-1 infection (Sastri et al., 2014, 2010). To test the hypothesis that this region undergoes dynamic conformational changes, we performed single-molecule Förster Resonance Energy Transfer (smFRET) experiments to monitor conformational changes in the CC-L2 dimer. Because the resonance energy transfer between donor and acceptor fluorophores is governed by the interfluorophore distance, smFRET is a powerful method to precisely measure conformational changes which occur in a protein. We observe that the WT rhTRIM5α dimer exhibits substantial conformational variability, exchanging among at least three conformations. Moreover, mutants which exhibited altered restriction exhibited altered occupancy of these FRET states as well as altered ability to transition between the states. Collectively, these results reveal that the rhTRIM5α dimer undergoes dynamic conformational changes and suggest a model where transitions between individual conformations might account for the ability of TRIM5α to induce the disassembly of CA assemblies.

2. Materials and methods

2.1. Recombinant DNA

To generate 6xHis-tagged CCL2 peptides, the CCL2 fragments WT rhTRIM5α and its L2 mutants (residues 132–296 of the full length protein) were cloned into the pET-15b vector by using the NdeI and BamHI restriction sites. To introduce a C-terminal cysteine on the CCL2 peptides, primers were generated against the C-terminal end of the CCL2 gene fragment containing the codon for cysteine and mutagenesis was performed by PCR mutagenesis.

2.2. Protein expression and purification

Transformed BL21(DE3) cells were grown in 0.25 l of Luria broth containing 100 μg/ml carbenicillin (Invitrogen) until the optical density at 600 nm (OD_{600}) reached 0.6. The bacterial cultures were then induced to express WT or L2 mutant rhTRIM5α CCL2 peptides by adding 1 mM isopropyl β-D-1- thiogalactopyranoside (IPTG) (Invitrogen) and shaking the cultures for 4 h at 37 °C. To purify 6xHis-tagged CCL2 peptides, bacterial pellets were lysed in a solution containing 50 mM Na_2HPO_4, 500 mM NaCl, 10 mM imidazole, 1% Triton X-100, 0.5 mg/ml lysozyme (Sigma), 8 M Urea, and a protease inhibitor cocktail (PIC) (Roche), followed by sonication. The lysates were then centrifuged at 13,000 rpm at 4 °C for 30 min. The pellet was discarded, and the supernatant was incubated with Talon metal affinity resin (Clontech) at 4 °C for 1–2 h with gentle mixing to facilitate binding of the His-tagged proteins to the resin. The mixture was passed through a 2-ml Talon disposable gravity column (Clontech) twice. The flow-through was discarded, and the resin was washed with a buffer

containing 50 mM Na_2HPO_4, 500 mM NaCl, and 8 M urea (pH 8.0). The 6xHis-tagged proteins were eluted from the resin by using an elution buffer (50 mM Na_2HPO_4, 500 mM NaCl, 8 M urea, 300 mM imidazole). The protein fractions were analyzed by Coomassie staining of SDS-PAGE gels, and the fractions with the highest purity were dialyzed at 4 °C in decreasing concentrations of Urea (4 M, 2 M, and 0 M) for 3 h or overnight per step using 10,000 MWCO Slid-A-Lyzer Dialysis Cassettes (Thermo). The proteins were then spun at 10,000 rpm at 4 °C for 30 min to remove aggregates and final protein concentrations were determined by measuring the absorbance at 280 nm.

2.3. Protein labelling

Purified proteins were incubated with TCEP at 10x the protein concentration at 4 °C 4 h or overnight to disrupt disulfide bonds. The proteins were then combined with a 3-fold excess of maleimide dye (Alexa Fluor 594 C5-maleimide or Alexa Fluor 488 C5-maleimide (Life Technologies)) in DMSO and incubated at 25 °C for 45 min. The reaction was incubated with 1 µl βME at 25 °C for 5 min to halt the labelling reaction. To separate free dye from protein, the sample was passed through a NAP-10 column (GE Healthcare) equilibrated with 50 mM sodium phosphate, pH 7, 1 mM DTT, 1.7 M $(NH_4)_2SO_4$ buffer. Proteins labelled with A488 or A594 flourophores were denatured in 8 M urea, mixed at a 1:1 ratio and urea was removed by serial dialysis to 4 M, 2–0 M urea in 50 mM Na-phosphate, pH 7.4, at 4 °C in the dark.

2.4. Glutaraldehyde cross-linking assay

Glutaraldehyde cross-linking assays were performed as previously described (Sastri et al., 2014). Briefly, labelled purified proteins were incubated with 0, 1, 2, and 4 mM glutaraldehyde for 5 min at room temperature. The glutaraldehyde was saturated by the addition of 1 M glycine. The cross-linked proteins were then subjected to SDS-PAGE using 4%-to-15% gradient Tris-HCl gels (Ready Gels; Bio-Rad) and subsequent imaging. Images of gels were acquired using a GE Typhoon Trio+ Gel Scanner using the 532 and 610 filters to image each fluorophore. The image was pseudo-colored and finished in Image Quant TL.

2.5. Single-molecule FRET measurements

Quartz slides were cleaned and passivated with maleimide-PEG containing 5% biotin-PEG to reduce non-specific surface adsorption and immobilize labelled protein, respectively (Lamichhane et al., 2015, 2010). A microfluidic chamber prepared from the passivated slides was washed with 0.2 mg/ml NeutrAvidin followed by incubation with 10 nM biotin conjugated penta-His antibody for 10 min. The chamber was then washed with imaging buffer (50 mM HEPES, 150 mM NaCl and 0.1 mg/ml BSA in 2 mM Trolox). The chamber was then incubated for 30 min with His-tagged, doubly labelled protein (100 nM) followed by multiple washes with imaging buffer to remove unbound protein. A 1 mM propyl gallate solution was introduced into the chamber as an oxygen scavenger as previously described (Berezhna et al., 2012).

smFRET data were acquired on a custom-built prism-type total internal reflection fluorescence microscope (Zeiss) using a 488 nm laser (Coherent) as an excitation source, described in detail previously (Berezhna et al., 2012). Fluorescence emission was collected by an inverted water-immersion objective with 1.2 NA (Zeiss), split into donor and acceptor channels using a Dual-View Imager device and imaged on an EMCCD camera (Andor Technology) (Berezhna et al., 2012; Lamichhane et al., 2013) with an integration time of 100 msec/frame. Movies were recorded with a custom data acquisition package and individual donor/acceptor intensity traces were extracted using IDL scripts (Ha lab, University of Illinois at Urbana Champaign).

2.6. Single-molecule FRET data analysis

Individual donor and acceptor intensity versus time traces were processed with custom Matlab software. Trajectories were corrected for 5% leakage of AlexaFluor 488 emission signal into the acceptor channel (determined previously) and background signal (determined from the average signal after photobleaching). Traces exhibiting single-step photobleaching and anti-correlated donor/acceptor signals were selected for further analysis. The apparent FRET efficiency, E, was calculated as $E=I_A/(I_A+I_D)$, where I_D and I_A are the corrected donor and acceptor emission intensity, respectively. Composite histograms of FRET efficiency were compiled from multiple traces and fit with up to three Gaussian distributions using IGOR Pro software (Version 6, WaveMetrics). Individual FRET traces were fit to a three-state Hidden Markov Model using the software HaMMy (McKinney et al., 2006). Transition density plots (TDP) (McKinney et al., 2006)were generated using custom Matlab scripts.

2.7. Molecular dynamics simulations

MD simulations were performed using GROMACS (Hess et al., 2008; Pronk et al., 2013) with the CHARMM 27 force field (Foloppe and MacKerell, 2000; MacKerell et al., 2004a, 2004b) and TIP3P water model (Jorgensen et al., 1983). We used a previously described model of the rhTRIM5a CCL2 dimer as a starting structure (Sastri et al., 2014) and truncated this model at residue 296 to model the recombinant proteins used in this study. The starting system was minimized using the steepest descent method for 1000 steps, and then was solvated in a rectangular water box of with a minimum of 20 Å from the surface of the protein to the edge of the solvent box. Na^+ and Cl^- ions were added to the solution to neutralize the charge of the system and to produce an ion concentration of 150 mM. The Particle Mesh Ewald (PME) method (Dardenet al., 1993; Essmann et al., 1995) was used to describe long-range electrostatic interactions. Molecular dynamics simulations were carried out with an integration time step of 2 fs. To reach the target temperature (300 K) and pressure (1 bar), the Berendsen method (Berendsen et al., 1984) was used with relaxation time of 0.1 ps. After a 100 ps equilibration. After that we created two additional systems with harmonic restrains to keep Cα atoms of C-terminal cysteines at specific distances which were observed by smFRET (51 Å, 68 Å), and allowed the secondary structural elements of the L2 region to relax during a 10 ns molecular dynamics simulation. Production simulations were performed in the NPT ensemble using the Nose-Hoover thermostat (Hoover, 1985; Nose and Klein, 1983) and a Parrinello-Rahman barostat (Nose, 1984; Parrinello and Rahman, 1981) with relaxation times of 1.0 ps.

3. Results

3.1. Determinants of restriction and assembly in the rhTRIM5α dimer

Our previous studies have examined the role that residues within the L2 region play in viral restriction (23). These studies collectively revealed two classes of mutants. Restriction-abrogating mutations, such as the RRV275-277AAA mutation, abrogate the ability of rhTRIM5α to inhibit HIV-1 infection (Fig. 2A and B). Conversely, restriction-enhancing mutations, such as the HKN271-273AAA mutation, exhibit inhibition of HIV-1 that is more potent than wt rhTRIM5α (Figs. 2A and B) (Sastri et al., 2014). Critically, circular dichroism analysis of the CC-L2 dimer revealed that the ability to inhibit HIV-1 correlated with the α-helical content of the dimer, such that mutations which abrogated HIV-1 restriction also exhibited reduced α-helical structure, while other mutations in the L2 region which increased the ability of rhTRIM5α to restrict HIV-1 exhibited more α-helical content than WT rhTRIM5α (Fig. 2B) (Sastri et al., 2014). However, mutations which abrogated restriction by disrupting α-helices in the L2 region

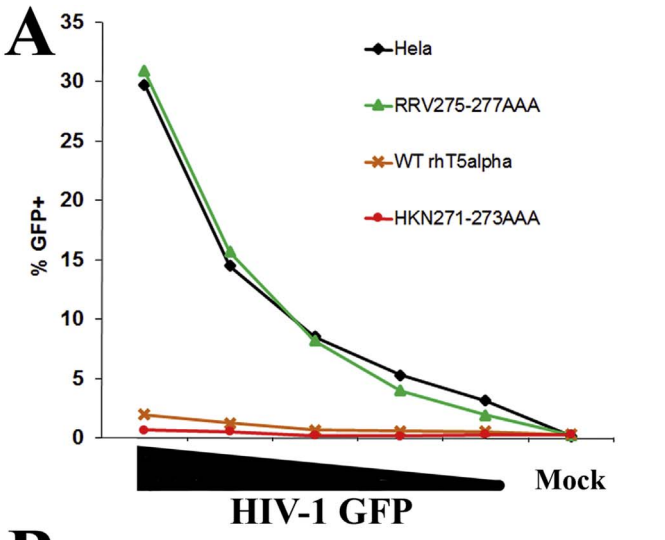

B

	Dimerization	% α-helix	HIV-1 Restriction	CA Binding
WT CC-L2	+	78%	++	+
HKN271-273AAA	+	87%	+++	+
RRV275-277AAA	+	68%	-	+

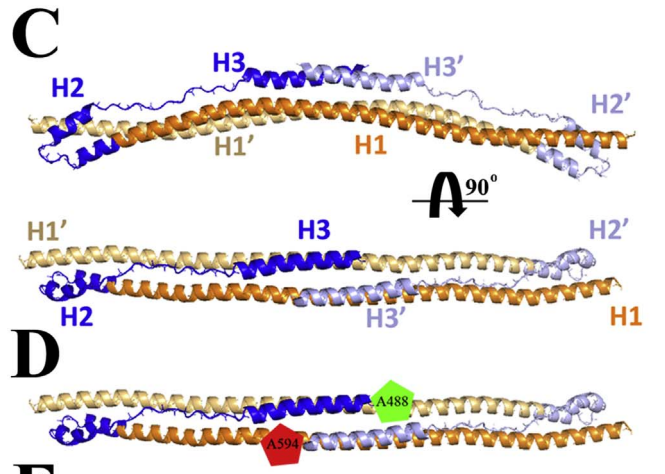

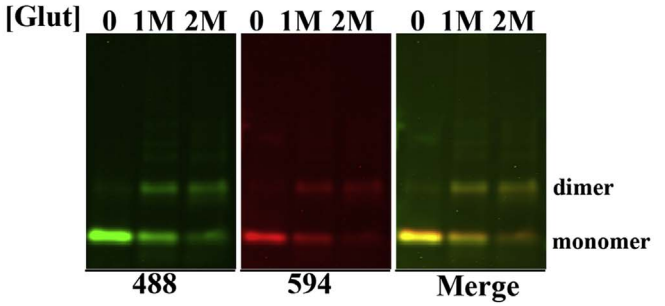

Fig. 2. Determinants of HIV-1 restriction within the L2 region of rhTRIM5α: A. Hela cells stably expressing rhTRIM5α were infected with serial dilution of HIV-1 GFP. GFP expression was measured 48 h after infection. B. Summary of the rhTRIM5α characteristics for WT and the indicated mutants, described in Sastri et al. (2014). Dimerization was assessed by glutaraldehyde crosslinking. % α-helicity was assessed using circular dichroism. Restriction was assessed as in A. CA binding was assessed by measuring co-precipitation with in vitro assembled CA. C. homology model of the rhTRIM5α CC-L2 dimer, similarly described in (Sastri et al., 2014). D. Location of fluorophore conjugation in dually labelled (A488, A594) rhTRIM5α dimers, as described in the text. E. Dually labelled rhTRIM5α dimers were crosslinked with 0, 1, or 2 mM glutaraldehyde for 5 min, subjected to electrophoresis and assessed via fluorescent imaging, as indicated. Results are representative of three or more individual experiments.

were still able to bind assembled CA tubes in vitro (Fig. 2B) (Sastri et al., 2014). Collectively, these results suggest that secondary structural elements in the L2 region contribute to the poorly understood effector function during restriction which drives the abortive disassembly of the viral core.

To understand how residues of the L2 region interact with residues of the CC domain in the context of the CC-L2 dimer, we generated a homology model of the rhTRIM5α CC-L2 dimer in which the rhTRIM5α sequence was threaded into the TRIM25 structure and the structure was allowed to relax during a 10 ns molecular dynamics simulation (Fig. 2C). For consistency, we have maintained the structural designations developed by Sanchez et al. (2014) to describe the three α-helices present in the TRIM25 dimer. The first helix, H1, spans the entire CC domain and a short stretch of residues of the L2 region. The second helix, H2, is a short helix which forms a hairpin structure with residues in H1. The last helix, H3, is located in the center of the dimer and is docked to H1 of the alternate monomer (H1′) (Fig. 2C). This homology model revealed putative interactions between the 275RRV277 motif present on H3 and an acidic 177DYD179 motif present on H1′ (and H1 and H3′). Given that disrupting this interaction through mutation of the RRV motif substantially reduced the helical content of the CC-L2 dimer (Fig. 2B) (Sastri et al., 2014), this also suggested to us that this interaction between RRV 275–277 and DYD177-179 promotes the formation of H3, and similarly predicted that the L2 region might alternate between helical, docked and unstructured, undocked conformations. To directly test this hypothesis, we introduced C-terminal cysteines into the CC-L2 dimer (Residues 132–296 in the native protein) to allow fluorescent labelling of these cysteines using maleimide chemistry (Fig. 2D). There are no cysteines in the native rhTRIM5α CC-L2 sequence, ensuring specific labelling of the cysteines at this location in the CC-L2 peptide. Purified recombinant protein containing an N-terminal HIS tag was labelled with either A488 or A594 fluorescent probes. The two pools of labelled protein were then denatured, mixed in a 1:1 ratio and allowed to renature to generate CC-L2 dimers containing both A488 and A594 fluorescent probes. Glutaraldehyde crosslinking revealed that the introduction of cysteines and subsequent fluorescent labelling did not disrupt the ability of the CC-L2 peptide to form dimers, which were the predominant species observed following crosslinking (Fig. 2E).

3.2. smFRET reveals dynamic conformational changes in the rhTRIM5α dimer

We next performed Total Internal Reflection Fluorescent (TIRF) microscopy on fluorescently labelled CC-L2 dimers to monitor dynamic conformational changes that might occur in these dimers. Following acquisition, we focused our analysis on individual, dually labelled dimers by analyzing traces that 1) exhibited single step photobleaching of the donor fluorophore during the acquisition period and 2) fluctuations in donor and acceptor fluorescence were anti-correlated. In this way, any dimers not labelled with both fluorophores, and protein aggregates or accumulations representing more than single, dually labelled dimers, were removed from the analysis. FRET traces from individual WT-CC-L2 dimers revealed fluctuations among three distinct FRET states indicating that, under these conditions, the CC-L2 dimer exchanges between three conformations (Fig. 3A). Composite FRET histograms were fitted to three Gaussian distributions centered at apparent FRET efficiencies of 0.2, 0.6, and 0.8 (Fig. 3B). These apparent FRET efficiencies correspond to interfluorophore distances of approximately 68 Å, 51 Å and 43 Å, respectively. This observation would not be expected if distal elements of the L2 region became transiently undocked from the CC helix, as we originally hypothesized. Rather, these data suggest that, on the time scale of these experiments, the L2 arms of the dimer remain in relatively close proximity while sampling three distinct conformations. The fractional populations of the fitted Gaussian distributions reveal that the lowest FRET state was

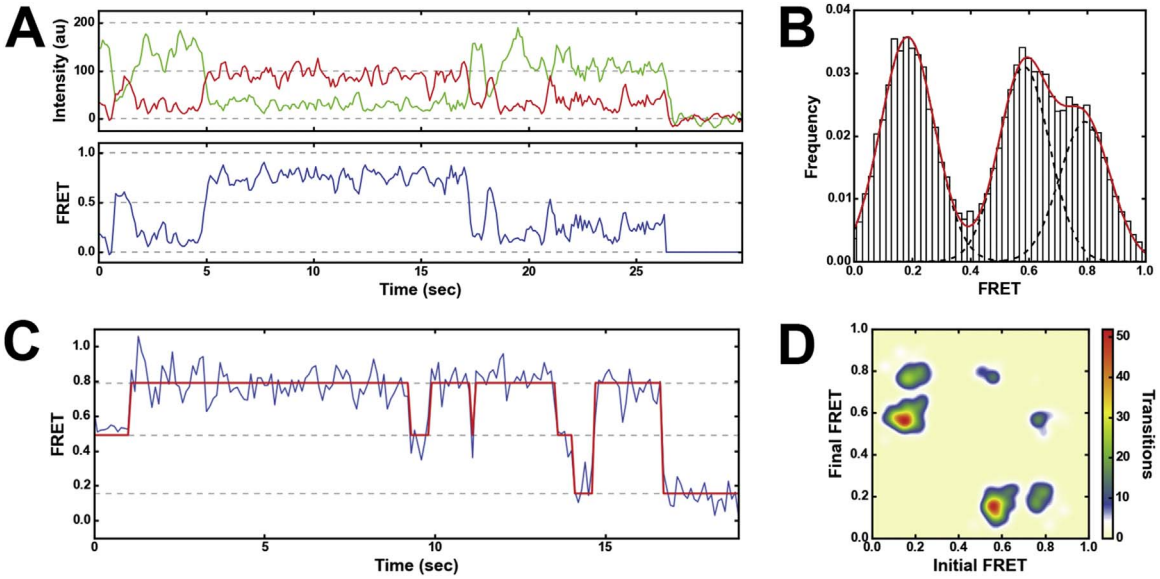

Fig. 3. Three conformational states are observed in the rhTRIM5α dimer: A. Representative fluorescence intensity (donor green, acceptor red) and FRET efficiency (blue) traces obtained from individual CC-L2 dimers via TIRF microscopy. B. A composite histogram of FRET efficiencies compiled from individual traces and fit to three Gaussian distributions centered around 0.2, 0.6 and 0.8 (dashed lines). The overall fit is shown as a red line. C. Idealized FRET traces were obtained by fitting each trace to a three state Markov Model. D. Transition density plot generated from the modeled FRET trajectories.

sample most frequently (42%), while the high-FRET state was occupied the least (24%) and the middle FRET state was occupied 34% of the time prior to photobleaching. These data reveal that the WT CC-L2 dimer undergoes spontaneous transitions between three distinct conformations.

Idealized FRET trajectories were generated by fitting individual FRET traces data to a three-state Hidden Markov Model (Fig. 3C). The fitted FRET efficiencies for each state were in good agreement with the mean FRET efficiencies determined from the cumulative histograms. The idealized trajectories were used to generate a transition density plot, revealing the connectivity of the individual FRET states (Fig. 3D, Table 1). The TDP reveals that transitions occur among all three conformations, with transitions between the 0.2 and 0.6 FRET states being the most common and transitions between the 0.8 and 0.6 FRET states being the least common. When the 0.6 FRET state was occupied, the protein was ~5 times more likely to transition to the 0.2 FRET state (279 transitions observed) than to the 0.8 FRET state (50 transitions observed) (Table 1). Transitions between the most extreme FRET states, without detectable occupancy of the middle FRET state, were also observed, and in the case of transitions from the 0.8 FRET state, transitions to the 0.2 FRET state was ~4 times more frequent than to the intermediate FRET state (150 transitions vs 36 transitions) (Table 1).

We next examined the conformations of CC-L2 dimers harboring mutations in the L2 region which either abrogate (RRV275-277AAA) or enhance (HKN271-273AAA) HIV-1 restriction by full length rhTRIM5α. The HKN271-273AAA mutation, which enhances restriction of rhTRIM5α (Sastri et al., 2014), existed preferentially in the 0.6 (51 Å) FRET state (64%), and sampled the 0.2 (68 Å) and 0.8 (43 Å) FRET state less frequently (31% and 5% respectively) than WT (Fig. 4A). Moreover, the rate of transitions between conformations was noticeably slower in this mutant compared to WT, preventing transition frequency calculation using Markov Modelling. In contrast, The RRV275-277AAA dimer exhibited constant and low FRET efficiency over time, existing almost entirely around the 0.2 (68 Å) FRET state (Fig. 4B) observed in the WT dimer. Our original hypothesis had suggested that the RRV275-277AAA mutant would be unable to establish contacts between the L2 region and CC domains necessary for stable docking of the L2 region to Helix 1, preventing the observation of discrete FRET states. These data, however, suggest stable docking between L2 and CC regions in this mutant. Taken together with the smFRET traces obtained for the HKN271-273AA mutant, these data suggest that the ability to assume the conformations associated with the 0.6 and 0.8 FRET states correlates to the ability to restrict HIV-1.

Table 1
Conformational transition frequency of rhTRIM5α CC-L2 dimer: the number of transitions between individual conformations observed by smFRET and identified using Markov Modelling between is shown.

N=118 (879 transitions)		Final state		
		0.2	**0.6**	**0.8**
Initial state	**0.2**	–	251 (28.6%)	113 (12.9%)
	0.6	279 (31.7%)	–	50 (5.7%)
	0.8	150 (17.1%)	36 (4.1%)	–

3.3. Molecular dynamics simulations of rhTRIM5α dimer conformations

We next used molecular dynamics simulations to establish models of the individual CC-L2 dimer conformations observed in our smFRET analysis. To generate these models, we used the TRIM25 homology model shown in Fig. 1A and introduced cysteine residues at the same position as our recombinant dimers (C297). To generate models for the observed FRET states, helices H3 and H3′ of this model were artificially separated by the observed separation distance by moving each cysteine an equivalent distance down the long axis of the dimer until the appropriate separation distance was achieved. H3 and H3′ were then artificially melted, after which the secondary structure in this region was allowed to reform in a 100 ns simulation (Fig. 5). In these models, the 68 Å separation model, which is the only conformation occupied by the RRV275-277AAA mutant, exhibited the least α-helical content in the residues which formed H3 in the 43 Å model. This is consistent with the observation that this mutant exhibits less α-helical content, as measured by circular dichroism (Fig. 2) (Sastri et al., 2014).

We also performed steered molecular dynamics (SMD) simulation in order to explore the mechanical/energetical properties of the transition between states, applying a spring constant of 600 kJ/mol/

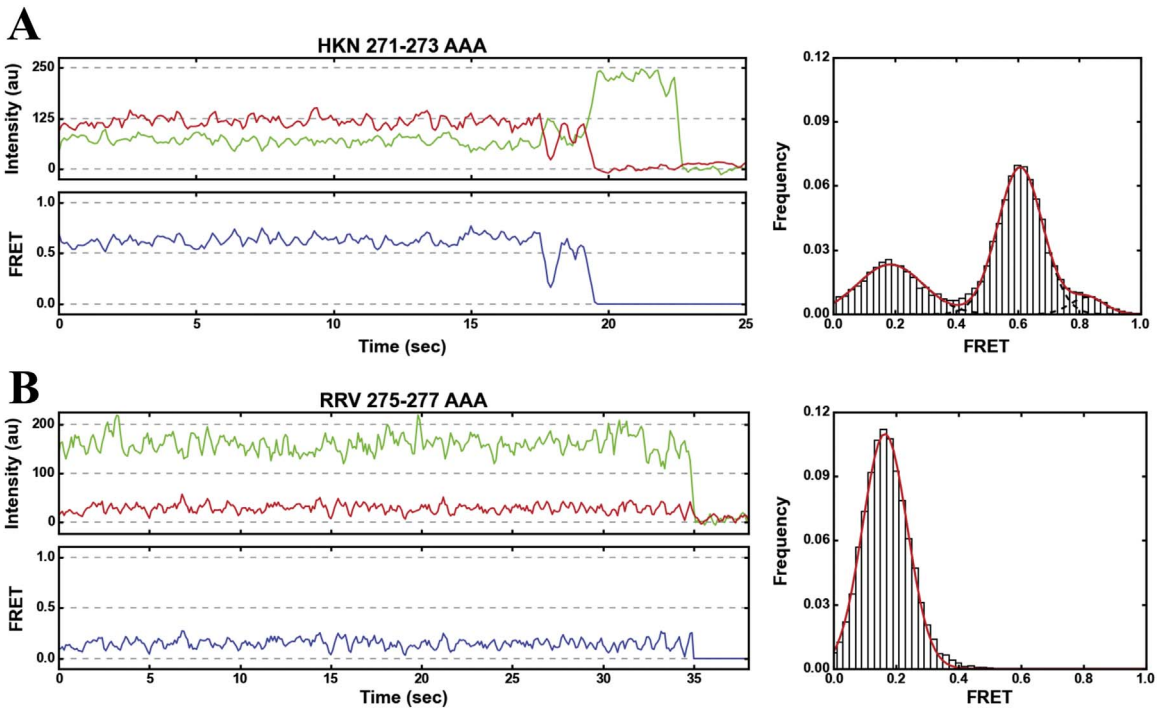

Fig. 4. Restricting enhancing or disrupting mutations in the CC-L2 region alter the stability of individual conformations of the rhTRIM5α dimer: A. Representative fluorescence intensity (donor green, acceptor red) and FRET efficiency (blue) traces obtained from individual HKN271-273AAA CC-L2 dimers via TIRF microscopy. A composite FRET histogram (right panel) compiled from individual traces was fit to three Gaussian distributions centered around 0.2, 0.6 and 0.8 (dashed lines). The overall fit is shown by the red line. B. Corresponding data for RRV275-277AAA CC-L2 dimers.

nm with a constant pulling velocity of 0.0015 nm/ps to the C-terminal cysteines, such that residues were pulled away from each other along the coil-coil region. As can be seen from Fig. 5B, drops in resistance force were observed were observed during the 1 ns SMD simulation, with drops corresponding to the loss of individual α-helical turns in the L2 region. Similar results were obtained when we performed a similar simulation using the original TRIM25 homology model containing residues 297–302 of the native protein. In these simulations, each drop in resistance force corresponded to 1–2 turns of the alpha-helix transitioning to a disordered coil (Fig. 5B). Collectively, this suggests that the secondary structure of H3 and H3' provides lateral force across the long axis of the dimer. Moreover, although this SMD examined the reduction of force associated with loss of secondary structural elements, it conversely supports the hypothesis that the formation of these secondary structural elements, as the dimer transitions from extended to compact conformations, is associated with the generation of lateral force along the same axis.

4. Discussion

In this study, we performed smFRET measurements to demonstrate dynamic conformational changes occurring in the basic dimeric unit of rhTRIM5α, comprising the CC-L2 domain. Other studies have utilized similar constructs to obtain structural information of TRIM family dimers, notably TRIM25 (Sanchez et al., 2014) and TRIM5α (Goldstone et al., 2014). Notably, the structures described in these two studies differed substantially with respect to their ability to resolve the structure of the L2 region. The structure of TRIM25 reveals two well-ordered α-helices (H3, H3′) which dock along the long axis of the CC domains to generate a 4 helix bundle (Sanchez et al., 2014). By contrast, the structure of TRIM5α failed to resolve precise coordinates of these residues in the dimer, although an antiparallel dimer similar to the TRIM25 dimer was clearly resolved (Goldstone et al., 2014). Additionally, the residues in which the TRIM5 structure failed to resolve residues in the L2 region are precisely those residues that our previous studies have implicated as governing HIV-1 restriction (Sastri et al., 2014, 2010). Given the dynamic conformational changes observed using smFRET in this study, it is not surprising that this region of the protein was not amenable to x-ray crystallography. Therefore, our studies may explain, in part, the results of Goldstone et al., and conversely, the studies of Goldstone et al. (2014) provide insight into which residues in the L2 region are contributing to the conformational variability observed in our smFRET experiments.

These studies, taken together with our previous in vivo studies examining how mutations in the L2 region influence restriction and secondary structure (Sastri et al., 2014, 2010), provide insight into the individual conformations assumed by rhTRIM5α. In our previous studies, we have found that residues in the L2 region govern the ability of rhTRIM5α to restrict HIV-1 infection (Sastri et al., 2014, 2010), finding that the ability of the CC-L2 domain to adopt α-helical structure correlated to its ability to restrict infection. Restriction-defective mutations, such as RRV275-277AAA, reduced the helical content of the dimer, while restriction enhancing mutations, such as HKN271-273AAA, exhibited more α-helical structure than WT protein. Here, we observe that the WT rhTRIM5α dimer exhibits frequent conformational transitions, which correlate to displacements of the L2 termini 25 Å relative to each other. Given that the RRV275-277AAA mutant exclusively assumed the more extended (68 Å) conformation, and has less α-helical content than the WT dimer (Sastri et al., 2014), this suggests that the 68 Å conformation has less α-helical secondary structure than the other two conformations observed in WT and the HKN271-273AAA mutant. By contrast, this suggests that the more compact conformations observed, in which the interfluorophore distance was 51 Å or 43 Å, have more α-helical content than the extended conformation. This was observed in our molecular dynamics simulations performed to understand the structural basis of these conformations (Fig. 5).

Although this study focused exclusively on the basic dimeric unit of rhTRIM5α, it is worth considering the impact these conformational changes in the CC-L2 region would have on the full length dimer. In

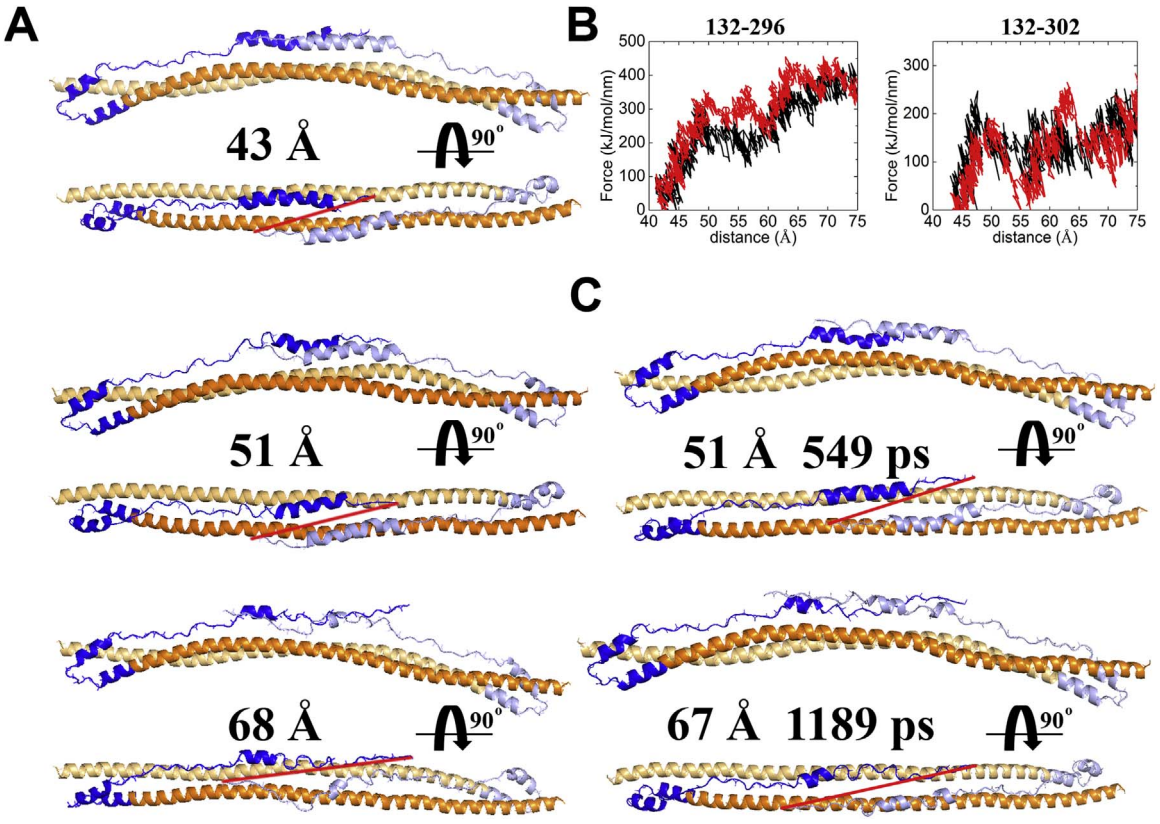

Fig. 5. Molecular dynamics simulations of FRET states assumed by the rhTRIM5α dimer: A. Molecular dynamics simulations were used to generate models of each FRET state observed experimentally. Individual cysteines were introduced after rhTRIM5α residue 296 in our previously described homology model of the rhTRIM5α dimer (Sastri et al., 2014). Individual models were generated by separating the C-terminal cysteines by the indicated distance along the long axis of the dimer and artificially melting H3 and H3′ and allowing the model to relax in a 100 ns simulation. The coiled coil domains are colored orange and light orange, while residues in the L2 region are labelled blue and light blue. B. Steered molecular dynamics simulations were used to generate force profiles resisting the pulling of the C-terminal cysteines along the axis of the dimer at constant velocity. Force profiles, plotted against the distance between C-terminal cysteines (top panel) or simulation time (bottom panel), using both the 43 Å model shown in A (residues 132–296) or a previously published homology model of the rhTRIM5α dimer incorporating residues 297–302, are shown. Force measured on each arm of the dimer are shown as black and red traces, respectively. C. Structural intermediates observed during the simulation shown in B, at the indicated time and separation distance between C-termini. The coiled coil domains are colored orange and light orange, while residues in the L2 region are labelled blue and light blue.

this context, the conformational transitions observed in the C-terminal portion of the L2 region are likely to affect the separation of the C-terminal SPRY domains which bind retroviral capsid assemblies. We speculate that this may be relevant to restriction via two distinct but not mutually exclusive mechanisms. First, variable spacing between SPRY domains may enhance the ability of TRIM5α proteins to bind a larger spectrum of CA assemblies with variably spaced binding sites. Second, SPRY translocation may drive the conserved ability of TRIM5α to disrupt the CA lattice during restriction (Stremlau et al., 2006; Zhao et al., 2011). In this regard, it has been observed that the minimal CA binding unit comprised of the CC-L2-SPRY domain of rhTRIM5α is sufficient to disrupt CA assemblies in vitro (Zhao et al., 2011). This suggests that the CA destabilizing activity is contained in this portion of the protein, even though no enzymatic activity has been ascribed to these domains of TRIM5α. The data here provide a biophysical explanation for this observation. If, for example, CC-L2-SPRY were to bind assembled CA in either of the more extended conformations we observe by smFRET, the transition to more compact conformations, driven by the formation of helices in the L2 region, may induce mechanical stress on the CA assembly. The dissipation of resistance force observed in our steered MD simulations as the C-terminal ends of the L2 region were pulled away from each other indirectly support this hypothesis. Considered in the opposite direction, the transition to more compact, alpha-helical states may similarly be associated with corresponding, transient increases in force. It is possible that this force may induce the translocation of the C-terminal SPRY domain following CA binding, which might be expected to induce mechanical stress on the CA lattice that induces premature disassembly. In support of this model, we and others have identified mutations in rhTRIM5α which abrogate restriction without affecting CA binding (Sastri et al., 2014, 2010; Yang et al., 2014). Specifically, the RRV-275-277AAA mutant can bind CA but fails to restrict HIV-1. The reduced α-helical content associated with this mutant (Fig. 1, Sastri et al., 2014), taken together with the fact that it exclusively occupies the more extended FRET state (Fig. 4) is consistent with a model where the formation of L2 helix 3 may act as a spring which triggers the displacement of the neighboring SPRY domain. MD simulations of the rhTRIM5α SPRY domain binding to assembled CA suggest that the SPRY domain can intercalate deep into the threefold interhexameric cleft (Kovalskyy and Ivanov, 2014), potentially providing leverage that translates SPRY domain translocation to disruption of the three fold axis, as observed by Zhao et al. (2011). Although additional studies are required to demonstrate that the conformational changes in the CC-L2 dimer observed by smFRET might actually drive the CA disassembly observed by Zhou et al., the data provided here demonstrate that smFRET is a valuable technique with which to assess the conformational changes that might occur in the context of rhTRIM5 dimers bound to assembled CA.

Acknowledgements

EC was supported by NIH grants AI093258, 5P50GM082545 and GM123538. DM was supported by 5P50GM082545. RL was supported by Postdoctoral Training Award (ID # F12-SRI-210) from the California HIV/AIDS Research program. SLR was supported by

1R01HL092321. This work used the Extreme Science and Engineering Discovery Environment (XSEDE), which is supported by National Science Foundation grant number ACI-1053575. This research was supported by equipment and facilities provided by National Institute of Health grant “Loyola Research Computing Core” 1G20RR030939.

References

Abe, H., Miyamoto, K., Tochio, N., Koshiba, S., Kigawa, T., and Yokoyama, S., 2007. Solution structure of the zinc finger, C3HC4 type (RING finger) domain of Tripartite motif-containing protein 5, In: RCSB PDB, RCSB.

Berendsen, H.J.C., Postma, J.P.M., Vangunsteren, W.F., Dinola, A., Haak, J.R., 1984. Molecular-dynamics with coupling to an external bat. J. Chem. Phys. 81 (8), 3684–3690.

Berezhna, S.Y., Gill, J.P., Lamichhane, R., Millar, D.P., 2012. Single-molecule Forster resonance energy transfer reveals an innate fidelity checkpoint in DNA polymerase. J. Am. Chem. Soc. 134 (27), 11261–11268.

Biris, N., Yang, Y., Taylor, A.B., Tomashevski, A., Guo, M., Hart, P.J., Diaz-Griffero, F., Ivanov, D.N., 2012. Structure of the rhesus monkey TRIM5alpha PRYSPRY domain, the HIV capsid recognition modul. Proc. Natl. Acad. Sci. USA 109 (33), 13278–13283.

Cai, C., Masumiya, H., Weisleder, N., Matsuda, N., Nishi, M., Hwang, M., Ko, J. K., Lin, P., Thornton, A., Zhao, X., Pan, Z., Komazaki, S., Brotto, M., Takeshima, H., Ma, J., 2008. MG53 nucleates assembly of cell membrane repair machinery, Nat. Cell Biol.

Campbell, E.M., Dodding, M.P., Yap, M.W., Wu, X., Gallois-Montbrun, S., Malim, M.H., Stoye, J.P., Hope, T.J., 2007. TRIM5 alpha cytoplasmic bodies are highly dynamic structure. Mol. Biol. Cell 18 (6), 2102–2111.

Darden, T., York, D., Pedersen, L., 1993. Particle Mesh Ewald – an N.Log(N) method for Ewald sums in large system. J. Chem. Phys. 98 (12), 10089–10092.

Diaz-Griffero, F., Qin, X.R., Hayashi, F., Kigawa, T., Finzi, A., Sarnak, Z., Lienlaf, M., Yokoyama, S., Sodroski, J., 2009. A B-box 2 surface patch important for TRIM5alpha self-association, capsid binding avidity, and retrovirus restrictio. J. Virol. 83 (20), 10737–10751.

Essmann, U., Perera, L., Berkowitz, M.L., Darden, T., Lee, H., Pedersen, L.G., 1995. A smooth Particle Mesh Ewald Method. J. Chem. Phys. 103 (19), 8577–8593.

Foloppe, N., MacKerell, A.D., 2000. All-atom empirical force field for nucleic acids: i. Parameter optimization based on small molecule and condensed phase macromolecular target data. J. Comput. Chem. 21 (2), 86–104.

Ganser-Pornillos, B.K., Chandrasekaran, V., Pornillos, O., Sodroski, J.G., Sundquist, W.I., Yeager, M., 2011. Hexagonal assembly of a restricting TRIM5alpha protei. Proc. Natl. Acad. Sci. USA 108 (2), 534–539.

Goldstone, D.C., Walker, P.A., Calder, L.J., Coombs, P.J., Kirkpatrick, J., Ball, N.J., Hilditch, L., Yap, M.W., Rosenthal, P.B., Stoye, J.P., Taylor, I.A., 2014. Structural studies of postentry restriction factors reveal antiparallel dimers that enable avid binding to the HIV-1 capsid lattic. Proc. Natl. Acad. Sci. USA 111 (26), 9609–9614.

Hess, B., Kutzner, C., van der Spoel, D., Lindahl, E., 2008. GROMACS 4: algorithms for highly efficient, load-balanced, and scalable molecular simulatio. J. Chem. Theory Comput. 4 (3), 435–447.

Hoover, W.G., 1985. Canonical dynamics – equilibrium phase-space distribution. Phys. Rev. A 31 (3), 1695–1697.

Jorgensen, W.L., Chandrasekhar, J., Madura, J.D., Impey, R.W., Klein, M.L., 1983. Comparison of simple potential functions for simulating liquid water. J. Chem. Phys. 79 (2), 926–935.

Kar, A.K., Mao, Y., Bird, G., Walensky, L., Sodroski, J., 2011. Characterization of a core fragment of the rhesus monkey TRIM5alpha protein, BMC Biochem., Vol. 12, p. 1.

Kovalskyy, D.B., Ivanov, D.N., 2014. Recognition of the HIV capsid by the TRIM5alpha restriction factor is mediated by a subset of pre-existing conformations of the TRIM5alpha SPRY domain. Biochemistry 53 (9), 1466–1476.

Lamichhane, R., Berezhna, S.Y., Gill, J.P., Van der Schans, E., Millar, D.P., 2013. Dynamics of site switching in DNA polymerase. J. Am. Chem. Soc. 135 (12), 4735–4742.

Lamichhane, R., Liu, J.J., Pljevaljcic, G., White, K.L., van der Schans, E., Katritch, V., Stevens, R.C., Wuthrich, K., Millar, D.P., 2015. Single-molecule view of basal activity and activation mechanisms of the G protein-coupled receptor beta2A. Proc. Natl. Acad. Sci. USA 112 (46), 14254–14259.

Lamichhane, R., Solem, A., Black, W., Rueda, D., 2010. Single-molecule FRET of protein-nucleic acid and protein-protein complexes: surface passivation and immobilization. Methods 52 (2), 192–200.

Langelier, C.R., Sandrin, V., Eckert, D.M., Christensen, D.E., Chandrasekaran, V., Alam, S.L., Aiken, C., Olsen, J.C., Kar, A.K., Sodroski, J.G., Sundquist, W.I., 2008. Biochemical characterization of a recombinant TRIM5alpha protein that restricts human immunodeficiency virus type 1 replication. J. Virol. 82 (23), 11682–11694.

Li, X., Yeung, D.F., Fiegen, A.M., Sodroski, J., 2011. Determinants of the higher order association of the restriction factor TRIM5{alpha} and other tripartite motif (TRIM) protein. J. Biol. Chem. 286 (32), 27959–27970.

Li, Y.L., Chandrasekaran, V., Carter, S.D., Woodward, C.L., Christensen, D.E., Dryden, K.A., Pornillos, O., Yeager, M., Ganser-Pornillos, B.K., Jensen, G.J., Sundquist, W.I., 2016. Primate TRIM5 proteins form hexagonal nets on HIV-1 capsid. Elife, **5**.

MacKerell, A.D., Feig, M., Brooks, C.L., 2004a. Extending the treatment of backbone energetics in protein force fields: limitations of gas-phase quantum mechanics in reproducing protein conformational distributions in molecular dynamics simulation. J. Comput. Chem. 25 (11), 1400–1415.

MacKerell, A.D., Feig, M., Brooks, C.L., 2004b. Improved treatment of the protein backbone in empirical force field. J. Am. Chem. Soc. 126 (3), 698–699.

McKinney, S.A., Joo, C., Ha, T., 2006. Analysis of single-molecule FRET trajectories using hidden Markov modeling. Biophys. J. 91 (5), 1941–1951.

Nose, S., 1984. A molecular-dynamics method for simulations in the canonical ensemble. Mol. Phys. 52 (2), 255–268.

Nose, S., Klein, M.L., 1983. Constant pressure molecular-dynamics for molecular-system. Mol. Phys. 50 (5), 1055–1076.

Ohkura, S., Yap, M.W., Sheldon, T., Stoye, J.P., 2006. All three variable regions of the TRIM5alpha B30.2 domain can contribute to the specificity of retrovirus restrictio. J. Virol. 80 (17), 8554–8565.

Ozato, K., Shin, D.M., Chang, T.H., Morse, H.C., 3rd, 2008. TRIM family proteins and their emerging roles in innate immunit. Nat. Rev. Immunol. 8 (11), 849–860.

Parrinello, M., Rahman, A., 1981. Polymorphic transitions in single-crystals – a new molecular-dynamics method. J. Appl. Phys. 52 (12), 7182–7190.

Pertel, T., Hausmann, S., Morger, D., Zuger, S., Guerra, J., Lascano, J., Reinhard, C., Santoni, F.A., Uchil, P.D., Chatel, L., Bisiaux, A., Albert, M.L., Strambio-De-Castillia, C., Mothes, W., Pizzato, M., Grutter, M.G., Luban, J., 2011. TRIM5 is an innate immune sensor for the retrovirus capsid lattic. Nature 472 (7343), 361–365.

Pronk, S., Pall, S., Schulz, R., Larsson, P., Bjelkmar, P., Apostolov, R., Shirts, M.R., Smith, J.C., Kasson, P.M., van der Spoel, D., Hess, B., Lindahl, E., 2013. GROMACS 4.5: a high-throughput and highly parallel open source molecular simulation toolkit. Bioinformatics 29 (7), 845–854.

Sanchez, J.G., Okreglicka, K., Chandrasekaran, V., Welker, J.M., Sundquist, W.I., Pornillos, O., 2014. The tripartite motif coiled-coil is an elongated antiparallel hairpin dime. Proc. Natl. Acad. Sci. USA 111 (7), 2494–2499.

Sastri, J., Campbell, E.M., 2011. Recent insights into the mechanism and consequences of TRIM5alpha retroviral restriction. AIDS Res Hum. Retrovir. 27 (3), 231–238.

Sastri, J., Johnsen, L., Smolin, N., Imam, S., Mukherjee, S., Lukic, Z., Brandariz-Nunez, A., Robia, S.L., Diaz-Griffero, F., Wiethoff, C., Campbell, E.M., 2014. Restriction of HIV-1 by rhesus TRIM5alpha is governed by alpha helices in the Linker2 region. J. Virol. 88 (16), 8911–8923.

Sastri, J., O'Connor, C., Danielson, C.M., McRaven, M., Perez, P., Diaz-Griffero, F., Campbell, E.M., 2010. Identification of residues within the L2 region of rhesus TRIM5alpha that are required for retroviral restriction and cytoplasmic body localization. Virology 405 (1), 259–266.

Stremlau, M., Owens, C.M., Perron, M.J., Kiessling, M., Autissier, P., Sodroski, J., 2004. The cytoplasmic body component TRIM5alpha restricts HIV-1 infection in Old World monkey. Nature 427 (6977), 848–853.

Stremlau, M., Perron, M., Lee, M., Li, Y., Song, B., Javanbakht, H., Diaz-Griffero, F., Anderson, D.J., Sundquist, W.I., and Sodroski, J., 2006. Specific recognition and accelerated uncoating of retroviral capsids by the TRIM5{alpha} restriction factor, Proc Natl Acad Sci USA.

Stremlau, M., Perron, M., Welikala, S., Sodroski, J., 2005. Species-specific variation in the B30.2(SPRY) domain of TRIM5alpha determines the potency of human immunodeficiency virus restrictio. J. Virol. 79 (5), 3139–3145.

Tareen, S.U., Emerman, M., 2011. Human Trim5alpha has additional activities that are uncoupled from retroviral capsid recognition. Virology 409 (1), 113–120.

Yamauchi, K., Wada, K., Tanji, K., Tanaka, M., Kamitani, T., 2008. Ubiquitination of E3 ubiquitin ligase TRIM5 alpha and its potential role. FEBS J. 275 (7), 1540–1555.

Yang, Y., Brandariz-Nunez, A., Fricke, T., Ivanov, D.N., Sarnak, Z., Diaz-Griffero, F., 2014. Binding of the rhesus TRIM5alpha PRYSPRY domain to capsid is necessary but not sufficient for HIV-1 restrictio. Virology 448, 217–228.

Yap, M.W., Nisole, S., Stoye, J.P., 2005. A single amino acid change in the SPRY domain of human Trim5alpha leads to HIV-1 restrictio. Curr. Biol. 15 (1), 73–78.

Yudina, Z., Roa, A., Johnson, R., Biris, N., de Souza Aranha Vieira, D.A., Tsiperson, V., Reszka, N., Taylor, A.B., Hart, P.J., Demeler, B., Diaz-Griffero, F., Ivanov, D.N., 2015. Ring dimerization links higher-order assembly of TRIM5alpha to synthesis of K63-linked polyubiquitin, Cell Rep.

Zhao, G., Ke, D., Vu, T., Ahn, J., Shah, V.B., Yang, R., Aiken, C., Charlton, L.M., Gronenborn, A.M., and Zhang, P., 2011. Rhesus TRIM5alpha disrupts the HIV-1 capsid at the inter-hexamer interfaces, PLoS Pathog, 7(3), e1002009.